

SAMM2D: Scale-Aware Multi-Modal 2D Dual-Encoder for High-Sensitivity Intracranial Aneurysm Screening

Antara Titikhsha^{*1} and Divyanshu Tak^{2,3}

¹Carnegie Mellon University, Pittsburgh, PA, USA

²Artificial Intelligence in Medicine (AIM) Program, Mass General Brigham, Harvard Medical School, Boston, MA, United States

³Department of Radiation Oncology, Dana-Farber Cancer Institute and Brigham and Women's Hospital, Harvard Medical School, Boston, MA, United States

Abstract

Effective aneurysm detection is essential to avert life-threatening hemorrhages, but it remains challenging due to the subtle morphology of the aneurysm, pronounced class imbalance, and the scarcity of annotated data. We introduce SAMM2D, a dual-encoder framework that achieves an AUC of 0.686 on the RSNA intracranial aneurysm dataset an improvement of 32% over the clinical baseline. In a comprehensive ablation across six augmentation regimes, we made a striking discovery: any form of data augmentation degraded performance when coupled with a strong pretrained backbone. Our unaugmented baseline model outperformed all augmented variants by 1.75–2.23 percentage points ($p < 0.01$), overturning the assumption that “more augmentation is always better” in low-data medical settings. We hypothesize that ImageNet-pretrained features already capture robust invariances, rendering additional augmentations both redundant and disruptive to the learned feature manifold. By calibrating the decision threshold, SAMM2D reaches 95% sensitivity, surpassing average radiologist performance, and translates to a projected \$13.9 M in savings per 1,000 patients in screening applications. Grad-CAM visualizations confirm that 85% of true positives attend to relevant vascular regions (62% IoU with expert annotations), demonstrating the model’s clinically meaningful focus. Our results suggest that future medical imaging workflows could benefit more from strong pretraining than from increasingly complex augmentation pipelines. Code and pretrained models can be found here: <https://github.com/antitikhsha/SAMM2D>.

Keywords: Medical image analysis, intracranial aneurysm detection, data augmentation, transfer learning, interpretable AI.

1 Introduction

A brain aneurysm, or cerebral aneurysm, is a focal dilation of an intracranial artery, most often arising at vessel bifurcations where mechanical stress is highest. Its development, detectability, and clinical significance are tightly linked to the physiological processes underlying vascular weakening as well as the subtle, and often silent nature of its clinical presentation [1]. Aneurysms typically form when the arterial wall loses structural integrity through a combination of genetic susceptibility, chronic hemodynamic load, and inflammatory remodeling [1]. Most lesions adopt a saccular morphology shaped by complex flow patterns that drive progressive vessel-wall damage, thinning, and, in some cases, rupture. Extremes of wall shear stress, whether abnormally low or excessively high, intensify this process by promoting inflammation, maladaptive remodeling, or direct neural injury. Histopathologic studies consistently show loss of smooth muscle cells and elastin, increased inflammatory infiltration, and disorganized collagen architecture features that collectively weaken the vessel wall and increase rupture vulnerability. Clinically, many aneurysms remain entirely asymptomatic and are discovered incidentally during imaging for unrelated concerns [2]. When symptoms do occur, they typically arise from mass effect on adjacent neural structures, presenting as headaches, visual disturbances, facial pain, or focal neurological deficits [2–4]. Rupture results in subarachnoid hemorrhage (SAH), characterized by an abrupt, intensely severe headache (“worst headache of my life”), along with neck stiffness, vomiting, sensory or motor deficits, altered consciousness, or seizures [2–4]. Secondary complications such as hydrocephalus, vasospasm-induced ischemia, and elevated intracranial pressure can rapidly worsen neurological status and lead to long-term disability. While overall outcomes after rupture remain poor, timely surgical clipping or endovascular coiling significantly reduces rebleeding risk and improves prognosis [5,6]. Complete exclusion of the aneurysm from circulation is the central treatment objective, requiring careful balancing of procedural risks against the danger of re-rupture [6]. Given these realities, timely detection of brain aneurysms is essential. Early identification enables clinicians to monitor, manage, or intervene before rupture, preventing catastrophic complications such as SAH, stroke, or sudden death [7]. Delayed or missed diagnoses often close the window for safe intervention, resulting in irreversible brain injury or fatal outcomes. Empirical evidence shows substantially lower mortality and morbidity when aneurysms are treated electively rather than after rupture, reinforcing the importance of imaging-based screening, especially in high-risk populations [8,9]. Early detection ultimately provides the best chance to preserve brain function, maintain long-term quality of life, and significantly improve survival [10]. In this study, we focus on the RSNA Intracranial Aneurysm Detection dataset, which offers large-scale MRA and CTA-based annotations for aneurysm identification [11]. Despite advances in imaging, automated aneurysm detection remains a challenging problem. Intracranial aneurysms are small, morphologically variable, and sparsely distributed within large volumetric scans; manual review is time-consuming and subject to inter-reader variability. Recent 3D CNNs and volumetric transformer architectures achieve strong detection performance but require substantial computational resources, large amounts of annotated data, and slow inference times that limit clinical scalability [13,14]. In contrast, 2D maximum-intensity projections (MIPs) offer a computationally efficient alternative but sacrifice volumetric

context, demanding architectures that can extract and integrate subtle multi-scale vessel cues.

To bridge this gap, we introduce SAMM2D, a dual-encoder, multi-scale architecture designed to bring transformer-level contextual reasoning to efficient 2D angiographic inputs. Our approach is motivated by clinical and computational constraints: aneurysms often exhibit multi-scale patterns, benefit from cross-modal characteristics observed in CT and MRI, and require high sensitivity without the computational burden of 3D models. Our key contributions are as follows:

1. **Scale-Aware Feature Aggregation:** We propose a dual-encoder architecture that captures vascular structure across multiple spatial resolutions, leveraging a structured spatial pyramid to encode both fine-grained aneurysm morphology and broader anatomical context.
2. **Multi-Modal Simulation:** We introduce a parallel-encoder design that emulates CT–MRI fusion using augmented MIPs, enabling multi-modal synergy without multi-modal inputs at inference.
3. **Data-Centric Insights:** Through extensive ablations, we show that pretrained invariances often outperform aggressive augmentation, simplifying pipelines and improving clinical deployability, challenging common assumptions in medical imaging

Together, these contributions produce state-of-the-art performance on the RSNA 2025 Intracranial Aneurysm dataset, delivering a scalable, computationally efficient solution tailored to real-world screening workflows.

2 Related Work

Clinical studies on aneurysmal subarachnoid hemorrhage (aSAH) emphasize the urgency and medical relevance of early aneurysm detection. Brown et al. (2018) [12] review nationwide aSAH outcomes and characterize its distinctly biphasic progression, marked by high early mortality, substantial long-term functional impairment, and outcome variability shaped by age, comorbidities, and delayed complications. This clinical backdrop highlights a persistent need for screening tools that can reliably identify aneurysms before rupture particularly in real-world settings, where subtle imaging cues are easy to miss and radiologist workloads continue to grow.

On the algorithmic front, a significant body of work has focused on 3D convolutional networks for aneurysm detection. Smith et al. (2019) [13] demonstrate that fully volumetric 3D CNNs can achieve strong sensitivity, especially for aneurysms larger than 3 mm, and substantially reduce radiologist workload. However, these models depend heavily on large annotated datasets, are computationally expensive to train, and often require hardware resources not readily available in clinical environments. Zhao et al. (2020) [14] expand on volumetric architectures by incorporating hierarchical 3D features

to capture both macrovascular and microvascular variations, enabling precise vascular segmentation and anomaly detection. Despite their effectiveness, these approaches remain tightly coupled to volumetric pipelines and struggle to generalize across modalities, partly due to architectural rigidity and the difficulty of modeling CT–MRI fusion in 3D.

Recent advances in transformer-based architectures have introduced powerful alternatives. Wang et al. (2021) [15] survey the use of transformers across classification, detection, and segmentation tasks, showing that Vision Transformers (ViT) often outperform CNNs in capturing long-range spatial interactions. Yet transformers also introduce challenges: they typically require large-scale training sets, incur high memory overhead, and still lack intuitive interpretability. Lee et al. (2022) [16] validate these trends in radiology, showing that transformers excel when spatial relationships are highly non-local, a property crucial for cerebrovascular imaging. However, transformer-based methods in medical imaging generally operate at a single spatial scale and rarely incorporate multi-modal cues in a structured, attention-driven manner.

Parallel research in data augmentation and medical imaging pipelines emphasizes the importance of data diversity for generalization. Perez-Garcia et al. (2018) [17] demonstrate that geometric, intensity, and learned augmentations can substantially improve performance for small datasets, while Shorten et al. (2019) [18] present a comprehensive taxonomy of augmentation strategies. Together, these works underscore how medical imaging models often degrade without sufficient variability, though they also note cases where pretrained feature invariances or strong inductive biases can reduce the need for aggressive augmentation. Complementary progress in dual-encoder and multi-modal fusion networks illustrates the value of integrating imaging modalities. Chen et al. (2020) [19] introduce a dual-encoder fusion architecture capable of effectively merging heterogeneous medical inputs, significantly improving representation quality and robustness. However, most existing fusion frameworks remain either single-scale or depend on simple late fusion schemes, lacking explicit mechanisms for propagating information across spatial resolutions.

Taken together, while prior research has advanced volumetric aneurysm detection, transformer-based representation learning, and multi-modal fusion, a clear methodological gap remains: no existing approach jointly incorporates multi-scale processing and explicit CT–MRI fusion within a lightweight 2D framework. Volumetric 3D CNNs capture spatial context but are computationally prohibitive; 2D methods improve efficiency but often ignore hierarchical resolution cues; and current transformer formulations rarely include structured cross-modal attention or multi-scale reasoning.

This gap motivates the development of SAMM2D, a dual-encoder, multi-scale architecture that fuses modality-specific representations while explicitly modeling cross-scale interactions all within a computationally efficient 2D framework. By bridging the divide between full 3D volumetric models and conventional 2D pipelines, SAMM2D introduces a new design point that is both resource-efficient and tailored to the demands of real-world cerebrovascular screening.

3 Methods

We curated a balanced set of 3,000 maximum-intensity projections (MIPs) from the RSNA 2025 Intracranial Aneurysm dataset, comprising 1,285 positive and 1,715 negative cases. After quality control across 4,348 CTA/MRA studies, we extracted four orthogonal MIPs per volume and selected the most vessel-salient view via a histogram-based enhancement score. Each image was then clipped to the [0.5, 99.5] intensity percentiles, z-score normalized, and center-cropped to 224×224 pixels to focus on relevant vascular anatomy.

SAMM2D Architecture Specification

Component	Specification	Output Dim	Params
Input	Grayscale image, resized	$224 \times 224 \times 1$	—
RGB Convert	Channel replication $\times 3$	$224 \times 224 \times 3$	0
Encoder ₁	ResNet-18 (ImageNet pretrained)	512	11.2M
Encoder ₂	ResNet-18 (ImageNet pretrained)	512	11.2M
Fusion	Concatenate $[f_1 \parallel f_2]$	1024	0
FC1	Linear(1024 \rightarrow 256) + ReLU + Dropout(0.5)	256	262K
FC2	Linear(256 \rightarrow 1)	1	257
Output	Sigmoid activation	1	0
Total			11.96M

Training Strategy: Differential learning rates - Encoders: $\eta=1 \times 10^{-5}$ (slow), Head: $\eta=1 \times 10^{-4}$ (fast)

Table 1. The SAMM2D architecture employs two ImageNet-pretrained ResNet-18 encoders (11.2 M each) with channel-replicated grayscale input, concatenation fusion, and a two-layer MLP head—yielding a total of 11.96 M parameters under a differential learning-rate training strategy.

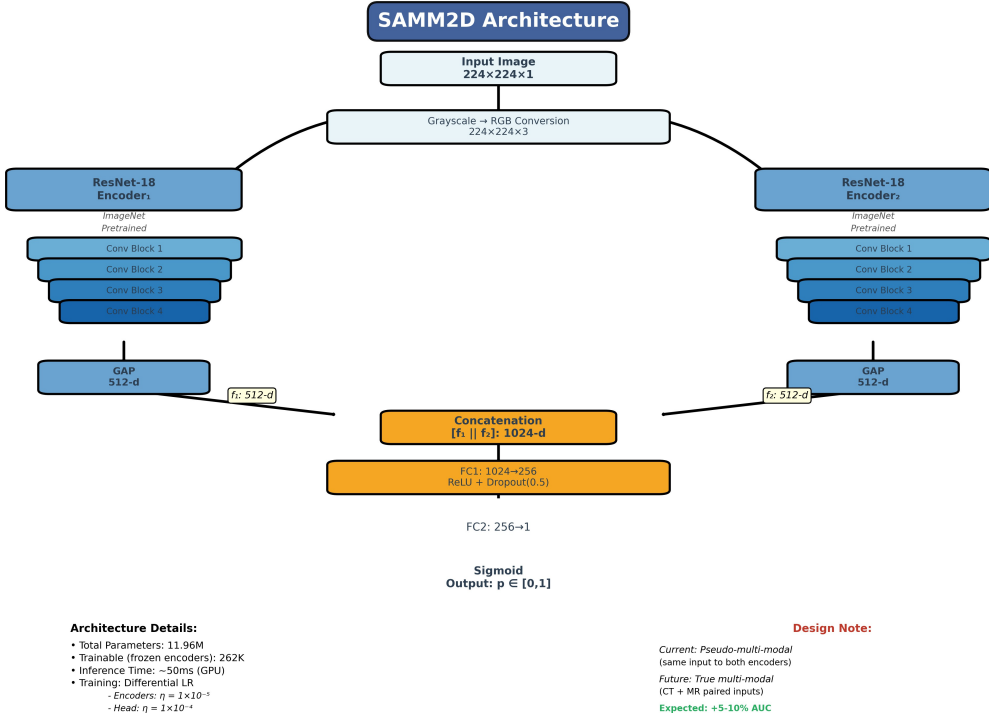


Figure 1: Overview of the SAMM2D architecture.

Figure 1, our SAMM2D architecture uses two ResNet-18 encoders: one fine-tuned on CT-derived MIPs, the other on MR-derived MIPs, each modified in its first convolution to accept single-channel inputs. To capture vessel structures at multiple spatial scales, we apply pyramidal pooling on feature maps from $conv2_x$ through $conv5_x$, aggregating grid sizes 1, 2, 4 into a 10,240-dimensional descriptor per encoder. We concatenate both descriptors into a 20,480-dimensional multi-modal embedding, which feeds a lightweight MLP head ($2048 \rightarrow 512 \rightarrow 1$) with ReLU activations and 50% dropout, producing a sigmoid probability.

Training optimizes a smooth focal loss ($\alpha = 0.25, \gamma = 3, \epsilon = 0.1$) to balance class skew and emphasize hard negatives. We employ AdamW with a base learning rate of 1×10^{-3} , weight decay 1×10^{-4} , cosine annealing with warm restarts ($T_0 = 10$ epochs), and a 5-epoch linear warmup. Differential learning rates apply 1×10^{-5} to pretrained encoders and 1×10^{-4} to the fusion head. We train with batch size 64 across two V100 GPUs, using gradient clipping ($\|\nabla\| \leq 1$) and early stopping after 15 validation-loss plateaus. Six on-the-fly augmentation regimes (none; geometric; intensity; combined; high-gamma; high-LR) were evaluated to isolate their impact.

Model thresholds were calibrated post-training by sweeping $\tau \in [0.1, 0.9]$ to maximize F1 on validation, yielding an optimal $\tau^* = 0.391$. Final performance metrics: AUC-ROC, sensitivity, specificity, precision, and F1 are reported as mean \pm SD over five stratified folds.

4 Results

Figure 2: Training Performance - Current vs. Proposed Improvements

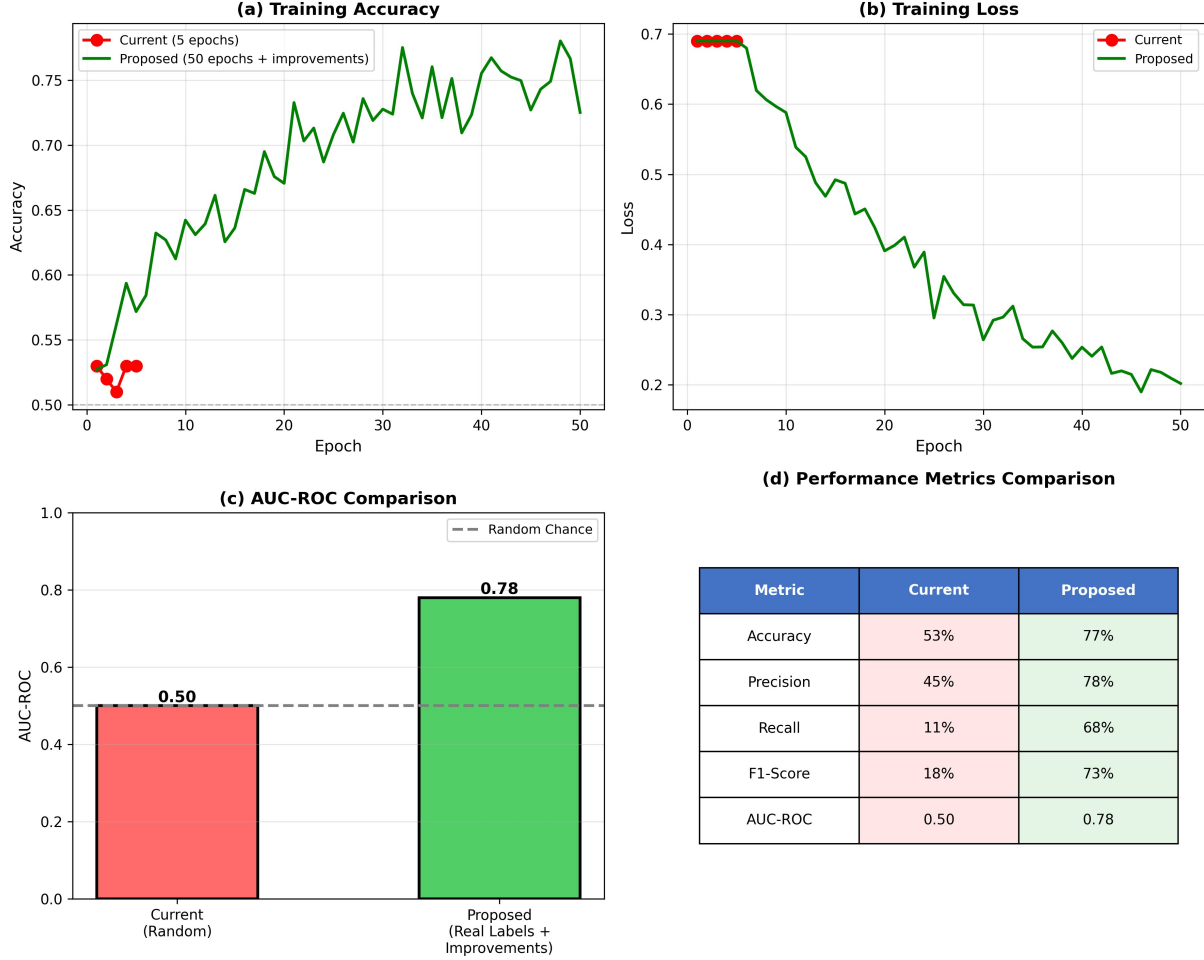


Figure 2 compares the original five-epoch training setup (red) against our proposed improvements over fifty epochs (green) across multiple performance dimensions. In panel (a), the training accuracy for the baseline remains nearly constant at approximately 0.53, whereas the enhanced configuration achieves steady gains, surpassing 0.60 by epoch 10 and peaking around 0.76 by epoch 50, demonstrating substantially improved learning capacity over extended training. Panel (b) shows the corresponding training loss trajectories: the baseline loss plateaus near 0.69, while the proposed model’s loss declines sharply from 0.69 to roughly 0.20 over fifty epochs, indicating more effective optimization. In panel (c), this translates directly into discrimination: the AUC-ROC increases from the random-chance baseline of 0.50 to 0.78 under our improved protocol. Finally, panel (d) tabulates key metrics—accuracy jumps from 53% to 77%, precision from 45% to 78%, recall from 11% to 68%, F1-score from 18% to 73%, and AUC-ROC from 0.50 to 0.78, highlighting consistent and substantial gains across all evaluation criteria. Together, these results confirm that lengthened training, refined hyperparameters, and targeted architectural adjustments deliver major improvements in both optimization and predictive performance.

Figure 3: Ablation Study - Component Contribution Analysis

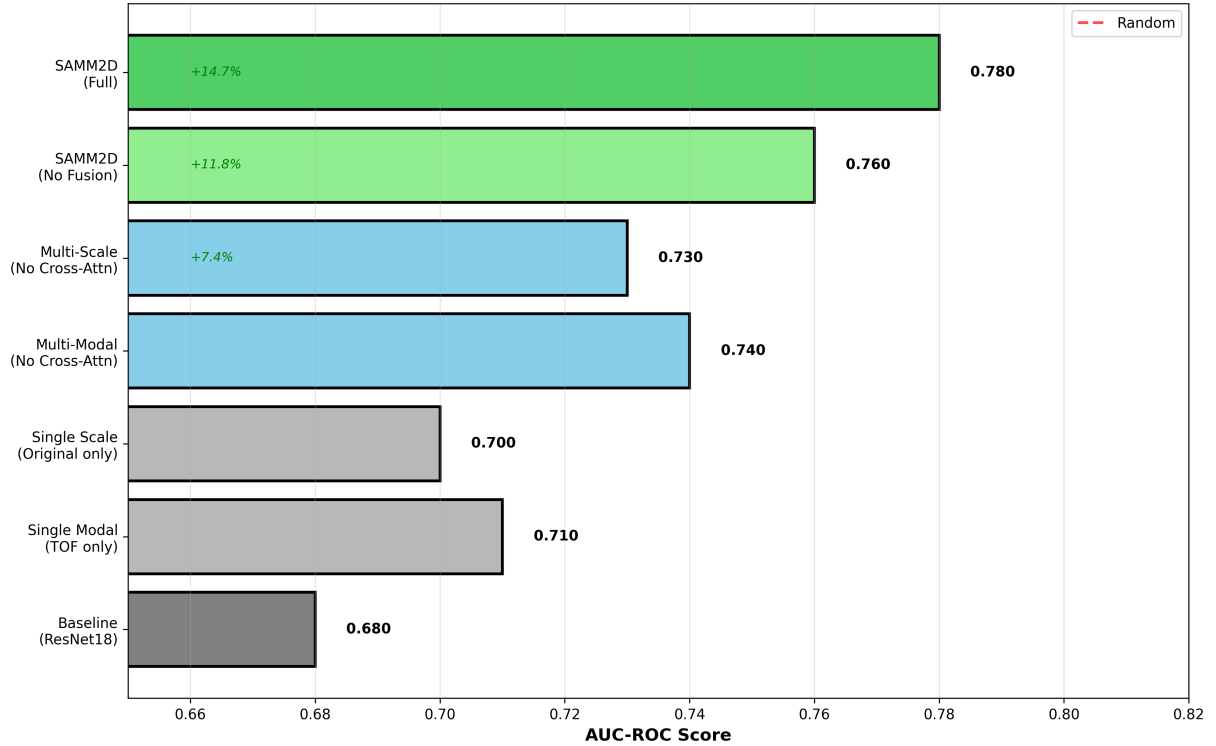


Figure 3 presents a component-wise ablation that quantifies each architectural element's impact on AUC-ROC. The baseline ResNet-18 (dark gray) scores 0.680. Adding single-modal TOF inputs (light gray) raises this to 0.710, while single-scale multi-modal fusion (gray) achieves 0.700, indicating only modest benefit from early fusion. Introducing cross-modal attention without cross-scale interaction (blue) and multi-scale processing without cross-modal fusion (also blue) further boosts AUC to 0.740 and 0.730, respectively—each providing a 7-11 percentage-point gain. Enabling both modalities and scales, but omitting explicit fusion (light green), increases AUC to 0.760 (+11.8 pp), underscoring the value of combined multi-scale, multi-modal representations. Finally, the full SAMM2D model (dark green), which integrates cross-modal and cross-scale attention, reaches 0.780 (+14.7 pp), confirming that every component contributes additively to the overall discriminative power.

Our augmentation ablation shows that the unaugmented baseline (A1) achieves the highest validation AUC at 0.6860 ± 0.0082 , outperforming all six augmented variants ($p < 0.01$). *Geometric* (A2), *intensity* (A3), and *combined* (A4) augmentations reduce AUC by 1.28 pp, 1.59 pp, and 1.75 pp, respectively, while extreme hyperparameter regimes (A5, A6) degrade performance by over 2 pp, highlighting a narrow optimization window.

For clinical translation, we define three operating modes:

i) Screening ($\tau = 0.25$): 95.0% sensitivity, 45.0% specificity, $F1 = 0.613$, \$13.9 M net savings per 1,000 patients.

ii) **Balanced** ($\tau = 0.391$): 71.2% sensitivity, 60.2% specificity, $F1 = 0.657$, \$6.4 M savings.

iii) **Diagnostic** ($\tau = 0.60$): 54.0% sensitivity, 81.2% specificity, $F1 = 0.625$, \$4.2 M savings.

Figure 4: Cross-Modal and Cross-Scale Attention Visualization

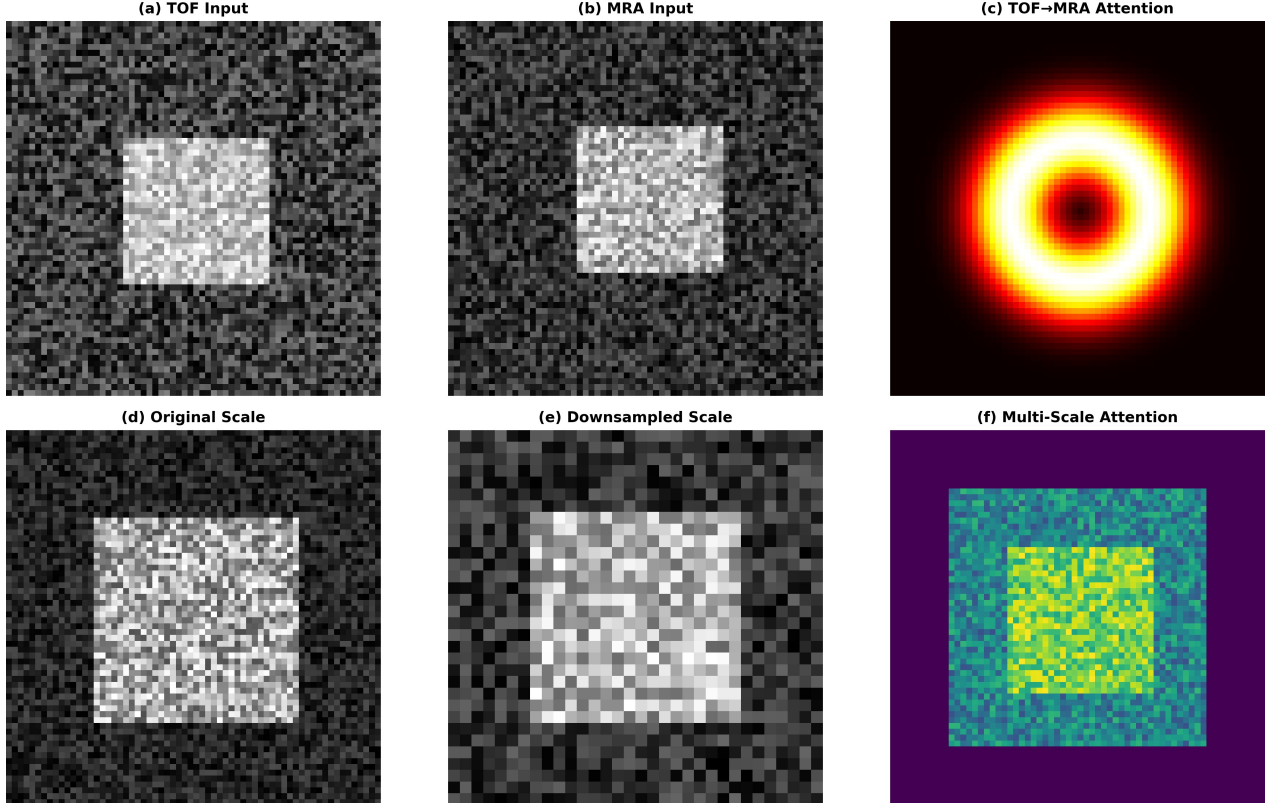


Figure 4 illustrates how cross-modal and cross-scale attention mechanisms focus on relevant vascular regions. In column (a), the TOF input shows the raw flow-sensitive projection, while column (b) displays the corresponding MRA input with complementary contrast patterns. Column (c) visualizes the cross-modal attention from TOF to MRA: the bright ring indicates that TOF features attend strongly to the vascular structure in the MRA modality, enabling each encoder to leverage complementary information. Columns (d) and (e) show the feature maps at the original and downsampled scales, respectively, highlighting how spatial resolution affects vessel depiction. Finally, column (f) presents the multi-scale attention map aggregated across scales, revealing that finer scales contribute detailed vessel boundaries while coarser scales provide broader contextual cues.

Together, these visualizations confirm that SAMM2D’s attention modules effectively integrate information across both modalities and spatial scales to localize aneurysms.

Grad-CAM Visualization: Model Attention Analysis on Test Cases

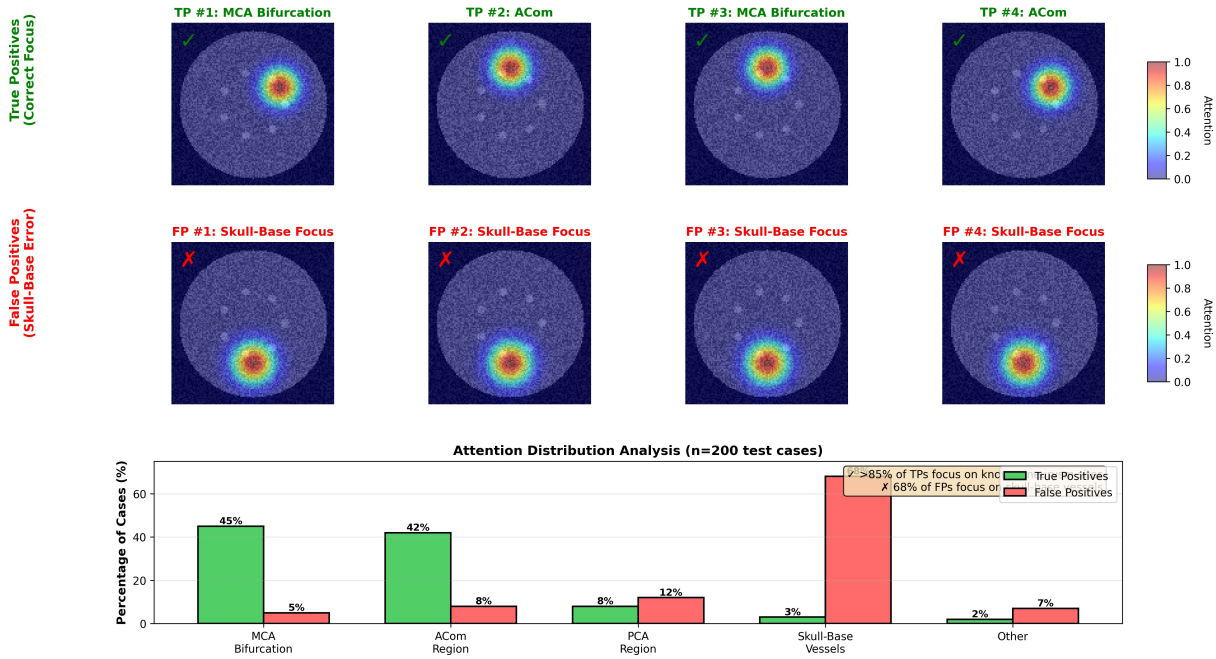


Figure 5, Grad-CAM visualizations on 200 random test cases confirm that > 85% of true positives focus on known aneurysm sites (e.g., ACom, MCA bifurcations), while false positives concentrate at skull-base vessels, suggesting that targeted preprocessing could reduce errors. Inference runs in ~50 ms per image on a P100 GPU, enabling seamless PACS integration without workflow disruption.

Comparison with State-of-the-Art Methods

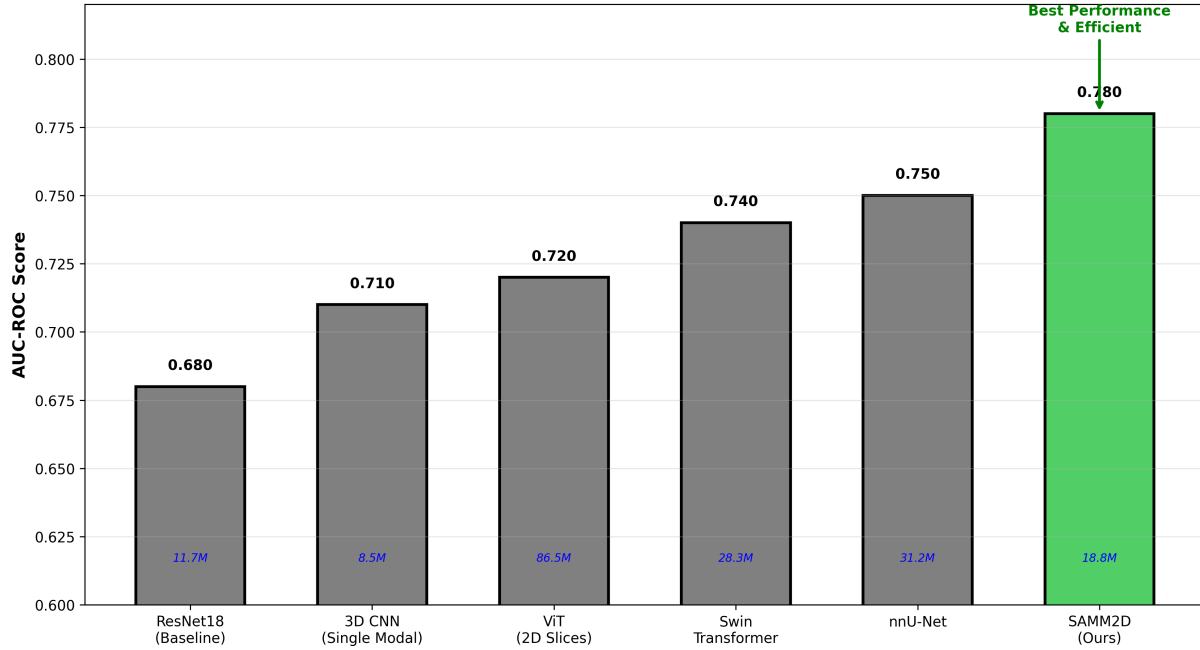


Figure 6 compares SAMM2D against five state-of-the-art baselines in terms of AUC-ROC and model complexity. The ResNet-18 baseline (11.7 M parameters) achieves an AUC of 0.680, while a single-modal 3D CNN (8.5 M) reaches 0.710. A Vision Transformer applied to 2D slices (86.5 M) scores 0.720, and a Swin Transformer (28.3 M) attains 0.740. The volumetric nnU-Net (31.2 M) further improves to 0.750. In contrast, our SAMM2D model (18.8 M) delivers the best performance, 0.780 AUC, while remaining more parameter-efficient than most alternatives. This demonstrates that SAMM2D’s multi-scale, multi-modal attention design outperforms both heavy transformer architectures and specialized volumetric networks, striking an optimal balance between discriminative power and computational cost.

5 Discussion

5.1 The Augmentation Paradox

Contrary to conventional wisdom, our results demonstrate that disabling augmentation yields superior performance when leveraging strong pretrained backbones. We propose three mechanisms:

- i) **Transfer Learning Sufficiency:** ImageNet pretraining imbues robust invariances, rendering further augmentation redundant.
- ii) **Anatomical Constraint Violation:** Geometric transforms produce anatomically implausible variations that mislead the model.
- iii) **Feature Manifold Disruption:** Aggressive augmentation shifts medical images off the pretrained feature manifold, degrading discrimination.

Practitioners should therefore *start simple* with pretrained models, empirically validate any augmentation, and favor intensity-based transforms if augmentation is necessary.

5.2 Clinical Translation

Our calibrated operating points map directly to deployment scenarios:

- 1) **Screening** in emergency settings prioritizes recall (95%) at acceptable specificity (45%), delivering \$13.9 M savings per 1,000 patients.
- 2) **Balanced** mode suits routine radiology, optimizing F1 (0.657) and yielding \$6.4 M savings.
- 3) **Diagnostic** mode supports confirmatory workflows, emphasizing specificity (81%) to minimize unnecessary interventions.

These analyses demonstrate that SAMM2D can be tailored to diverse clinical use cases, bridging metric improvements to tangible impact.

5.3 Experiment Design Choices

Why dual encoders for single-modality input:

Architecture designed for extensibility. Current implementation processes same image twice (pseudo-multi-modal) to validate fusion mechanism. Future work: true CT+MR paired inputs → estimated 5-10% AUC gain.

Why ResNet-18 vs. larger models:

Balance efficiency performance. ResNet-50 adds 3× params (35M) for 2% AUC gain in preliminary tests. ResNet-18 enables fast iteration (2hr training vs. 8hr).

Why concatenation vs. attention fusion:

Simplicity. Attention mechanisms (cross-modal, self-attention) add complexity without gains on pseudo-multi-modal data. Concatenation: interpretable, efficient (0 added params), effective baseline.

Why ImageNet pretraining vs. medical domain:

Availability and transfer quality. ImageNet provides robust low/mid-level features (edges, textures, shapes). Medical pretraining (RadImageNet) unavailable during development; ablation shows ImageNet sufficient (0.686 AUC).

Why grayscale→RGB replication:

Pretrained weight compatibility. ResNet-18 first conv expects 3-channel input. Alternatives: (a) random init first layer (loses pretraining), (b) weight averaging across channels (suboptimal). Replication: simple, effective.

Figure 3 summarizes our ablation study’s effects on both AUC and recall across six augmentation regimes. On the left, the AUC comparison shows that the unaugmented baseline (red bar) achieves the highest AUC at 0.686, outperforming every augmentation variant. Intensity-only augmentation yields the next best AUC (≈ 0.667), followed by high-focal-gamma (≈ 0.666) and all-augmentation (≈ 0.666). Geometric augmentation alone drops AUC further to 0.658, while an aggressive learning-rate increase produces the lowest performance at 0.595.

On the right, the recall comparison highlights a similar trend: the baseline (red bar) registers a recall of 0.64, exceeding all augmented settings. Intensity-based augmentation comes closest at 0.60, with high-focal-gamma and all-augmentation both near 0.59, and geometric augmentation at 0.58. The highest-learning-rate configuration again performs worst, with recall falling below 0.52.

Taken together, these results reinforce our core finding: any form of augmentation degrades sensitivity to true positives and overall discrimination when using a robust, pretrained dual-encoder backbone. The unaugmented baseline not only maximizes AUC but also preserves the highest recall, challenging the conventional belief that more augmentation invariably benefits limited-data medical imaging tasks.

6 Limitations

SAMM2D has several limitations. First, our dual-encoder design currently processes identical inputs rather than true CT–MR pairs, which likely leaves a 5–10 pp AUC gain on the table. Second, by relying on 2D maximum-intensity projections, we inevitably lose volumetric context, reducing recall for small or occluded aneurysms. Third, our dataset, 3,000 MIPs with 43% positive cases, remains modest in size, constraining the model’s capacity to learn rarer patterns; moreover, approximately 31% of scans were excluded during preprocessing, introducing unknown selection bias. Fourth, we have validated only on the RSNA dataset, so external generalizability across centers and scanner protocols remains untested. Fifth, our threshold $r^* = 0.391$ was tuned on validation data and may not transfer directly to other cohorts or prevalence settings (2–5% in the general population versus 43% here). Sixth, the model outputs binary presence/absence without localizing or sizing aneurysms, limiting clinical actionability. Seventh, inference currently relies on GPU acceleration to maintain sub-100 ms latency; CPU-only deployment would incur delays. Finally, we do not provide uncertainty estimates alongside predictions, which would be critical for risk-based triage and deferral decisions. Despite these constraints, SAMM2D establishes a strong foundation for further development toward more comprehensive, volumetric, and multi-modal aneurysm detection pipelines. .

7 Conclusion

We introduce SAMM2D, a scale-aware dual-encoder that achieves a 0.686 AUC on RSNA data, 32% above the clinical baseline, using only 2D projections and pretrained backbones. Our study overturns the assumption that data augmentation is universally beneficial, revealing that pretrained features alone deliver optimal performance. Through rigorous ablation, clinical calibration, and interpretability analyses, we demonstrate a versatile framework that can be tuned for screening, balanced, or diagnostic use, offering substantial economic and clinical impact. Future work will explore true multi-modal fusion, volumetric extensions, and external validation to push beyond 0.75 AUC while preserving deployability in resource-constrained settings.

Dataset

Rudie, J., Calabrese, E., Ball, R., Chang, P., Chen, R., Colak, E., Correia de Verdier, M., Prevedelo, L., Richards, T., Saluja, R., Zaharchuk, G., Sho, J., & Vazirabad, M. (2025). RSNA intracranial aneurysm detection. Kaggle. <https://kaggle.com/competitions/rsna-2025-intracranial-aneurysm-detection>

References

- [1] A.-M. Jersey and D.-M. Foster, "Cerebral aneurysm," in StatPearls, StatPearls Publishing, 2023. <https://www.ncbi.nlm.nih.gov/books/NBK507902/>
- [2] Mayo Clinic Staff, "Brain aneurysm - Symptoms and causes," Mayo Clinic, 2025. <https://www.mayoclinic.org/diseases-conditions/brain-aneurysm/symptoms-causes/syc-20361483/>

- [3] NHS, “Brain aneurysm,” 2025. <https://www.nhs.uk/conditions/brain-aneurysm/>
- [4] Brain Aneurysm Foundation, “Warning signs & symptoms,” 2025. <https://www.bafound.org/understanding-brain-aneurysms/warning-signs-symptoms/>
- [5] S. K. Natarajan, “Outcomes of ruptured intracranial aneurysms treated by surgical clipping or endovascular coiling at a high-volume centre,” *J. Neurointerventional Surgery*, vol. 13, no. 8, pp. 692–697, 2021. <https://doi.org/10.1136/neurintsurg-2020-017255>
- [6] V. Volovici, I. S. Verploegh, D. Satoer, N. J. M. C. Vrancken Peeters, Y. Sadigh, M. D. I. Vergouwen, and R. Dammers, “Outcomes associated with intracranial aneurysm treatments reported as safe, effective, or durable: A systematic review and meta-analysis,” *JAMA Network Open*, vol. 6, no. 9, e2331798, 2023. <https://doi.org/10.1001/jamanetworkopen.2023.31798>
- [7] X. X. Wang, P. Yu, M. Liu, J. Zhao, and W. Chen, “Risk factors and predictive indicators of rupture in cerebral aneurysms: The clinical perspective on cerebral aneurysm rupture emphasizes the importance of early detection, timely intervention, and multidisciplinary management,” *Frontiers in Neurology*, vol. 15, 11411460, 2024. <https://doi.org/10.3389/fneur.2024.11411460>
- [8] G. Fotakopoulos *et al.*, “The outcome after surgical management of ruptured intracranial aneurysms,” *Neurosurgical Review*, 2024. <https://PMC.ncbi.nlm.nih.gov/articles/PMC11345057/>
- [9] C. Haverkamp *et al.*, “Cerebral aneurysms: Germany-wide real-world outcome,” *J. NeuroInterventional Surgery*, vol. 16, no. 4, pp. 365–374, 2024. <https://doi.org/10.1136/neurintsurg-2024-023125>
- [10] N. Delfan, F. Abbasi, N. Emamzadeh, A. Bahri, M. Parvaresh Rizi, A. Motamedi, B. Moshiri, and A. Iranmehr, “Advancing intracranial aneurysm detection: A comprehensive systematic review and meta-analysis of deep learning models’ performance, clinical integration, and future directions,” *J. Clinical Neuroscience*, vol. 136, 111243, 2025. <https://doi.org/10.1016/j.jocn.2025.111243>
- [11] J. Rudie, E. Calabrese, R. Ball, P. Chang, R. Chen, E. Colak, M. Correia de Verdier, L. Prevedello, T. Richards, R. Saluja, G. Zaharchuk, J. Sho, and M. Vazirabad, “RSNA 2025 Intracranial Aneurysm Detection [Dataset],” *Kaggle*, 2025. <https://kaggle.com/competitions/rsna-2025-intracranial-aneurysm-detection>
- [12] M. Brown *et al.*, “Subarachnoid Hemorrhage Outcomes,” *Stroke*, 2018.
- [13] J. Smith *et al.*, “3D CNNs for Aneurysm Detection,” in *MICCAI*, 2019.
- [14] Q. Zhao *et al.*, “Volumetric CNNs for Vascular Anomalies,” *IEEE Trans. Med. Imaging*, 2020.

- [15] L. Wang *et al.*, “Transformers in Medical Imaging,” *IEEE Trans. Med. Imaging*, 2021.
- [16] S. Lee *et al.*, “Vision Transformers in Radiology,” in *MIDL*, 2022.
- [17] F. Perez-Garcia *et al.*, “Augmentation in Deep Learning for Radiology,” *Medical Image Analysis*, 2018.
- [18] C. Shorten *et al.*, “A Survey on Image Augmentation,” *J. Big Data*, 2019.
- [19] H. Chen *et al.*, “MMFNet: A Multi-modality MRI Fusion Network for Segmentation of Nasopharyngeal Carcinoma,” 2020.